Observations and analysis of an urban boundary layer during extreme heat events

Gabriel Rios [1*, 2*], Prathap Ramamurthy [1, 2], Mark Arend [2, 3]

1. Department of Mechanical Engineering, CUNY City College, New York, New York
2. NOAA Center for Earth System Sciences and Remote Sensing Technologies, New York, New York
3. Department of Electrical Engineering, CUNY City College, New York, New York

Corresponding author: Gabriel Rios (grios001@citymail.cuny.edu)

*** Current affiliation(s)**: Department of Mechanical Engineering, CUNY City College, New York, New York; NOAA Center for Earth System Sciences and Remote Sensing Technologies, New York, New York

For submission to the Quarterly Journal of the Royal Meteorological Society.
Last updated: February 1, 2022.

Abstract

Extreme heat presents a significant risk to human health and infrastructure in cities. Several studies have been conducted in the past two decades to understand the interaction between the synoptic-scale extreme heat events and local-scale urban heat island effects. However, observations of boundary layer characteristics during these periods have been relatively rare. Our current understanding of boundary layer dynamics is incomplete, particularly in coastal urban environments where the local climatology is highly influenced by land-sea thermal gradients. Here we analyze the evolution and structure of the urban boundary layer during regular and extreme heat periods. Our primary goal is to understand how boundary layer dynamics during extreme heat events regulate near-surface transport of mass, momentum, and heat. The analysis will also focus on how the urban surface layer interacts with the mixed layer during these events. Our analysis focuses on the New York City metropolitan area and relies on observations from vertical profilers (Doppler lidar, microwave radiometer) and quantities derived by analytical methods. Additionally, satellite and reanalysis data are used to supplement observational data.

1 Introduction

Extreme heat poses a major risk to life and property. The effects of extreme heat are expected to impact cities especially, which presents a significant hazard for vulnerable populations and infrastructure. With regards to effects on public health, studies have shown that extreme and prolonged heat increases mortality and exacerbates existing health conditions in high-risk populations (Anderson and Bell, 2011; Frumkin, 2016; Heaviside, Macintyre, and Vardoulakis, 2017; Madrigano et al., 2015). With regards to effects on infrastructure, studies have shown that extreme heat subjects networks critical to urban areas (e.g., electrical grid, public transportation) under significant stresses and/or failure (McEvoy, Ahmed, and Mullett, 2012; Zuo et al., 2015). These events are projected to increase in frequency due to the effects of climate change. Projections indicate that the impacts of future climate will cause adverse effects of extreme heat to become more frequent and severe (Burillo et al., 2019; Forzieri et al., 2018; Peng et al., 2011).

The meteorology of extreme heat events and its impacts on urban areas can be observed from the synoptic and local scales. From a synoptic scale, extreme heat events are often caused by the sustained presence of a high-pressure system over an area, resulting in lower wind speeds and warm air subsidence, promoting higher surface temperatures (Black et al., 2004; Miralles et al., 2014). From a local perspective, the amplified impact of extreme heat events on cities is a result of the urban heat island (UHI) effect, which occurs as a result of the modification of land surface properties due to the built environment. The modification of surface properties has been shown to increase near-surface air temperatures due to factors such as radiation entrapment, increased heat storage, and lower evapotranspirative cooling (Chen, Yang, and Zhu, 2014; Li and Elie Bou-Zeid, 2013; Ramamurthy and Bou-Zeid, 2017; Zhao et al., 2018). Additionally, urban areas near large bodies of water experience effects from the sea breeze, which has been shown to play a moderating influence on the intensity of the UHI effect (Hu and Xue, 2016; Jiang et al., 2019; Stéfanon et al., 2014).

The processes on these two scales can be connected by understanding the structure and dynamics of the urban boundary layer (UBL), which is the lowest part of the troposphere in which surface-atmosphere exchanges occur that directly affect human activity. There have been a large number of numerical studies performed to improve our understanding of UBL processes during extreme heat events, which have been important for conceptualizing the role of synoptic-scale and surface forcings on urban climate. However, in-depth observational analyses of UBL structure and dynamics are limited, which has

This study attempts to use observations and analytical methods to provide insight into the following questions:

1. How does the UBL differ from the climatology during extreme heat events?
2. How does UBL structure change with regards to atmospheric stability?
3. How do turbulent properties differ between sites in the same urban area?
4. How does the sea breeze affect UBL properties during normal conditions and extreme heat events?

2 Data collection and analysis

2.1 Study site

The UBL over New York City is observed and analyzed in this study. Observational data was captured at four locations within New York City (Table 1).

Table 1: Locations and details of observations sites.

	Bronx	Manhattan	Queens	Staten Island
Coordinates	40.87248°N, -73.89352°E	40.82044°N, -73.94836°E	40.73433°N, -73.81585°E	40.60401°N, -74.14850°E
Elevation (m a.g.l.)	57.8	90.6	56.3	32.4
Element roughness height (m a.g.l.)				
Instruments used	Lidar, microwave radiometer	Lidar, sonic anemometer	Lidar, microwave radiometer, sonic anemometer	Lidar, microwave radiometer, sonic anemometer
Valid wind directions	N/A	120 to 300°	180 to 360°	None

2.2 Observational instruments

Observations of the UBL were made using a synthesis of microwave radiometers, lidars, sonic anemometers, and surface weather stations.

Vertical profiles of temperature and vapor density were captured using microwave radiometers (Radiometrics MP-3000A). Profiles are captured at 58 height levels starting at 50 m and ending at 10 km above ground level, with vertical steps of 50 m from 50 to 500 m, 100 m from 500 m to 2 km, and 250 m steps above 2 km.

2.2.1 Data availability

2.3 Derived quantities

3 Results

3.1 Mean and turbulent boundary layer properties

3.2 Normal and extreme heat boundary layer properties

3.3 Effects of the sea breeze circulation

4 Discussion

5 Conclusions

References

Anderson, G Brooke and Michelle L Bell (2011). "Heat waves in the United States: mortality risk during heat waves and effect modification by heat wave characteristics in 43 US communities". In: *Environmental health perspectives* 119.2, pp. 210–218.

Black, Emily et al. (2004). "Factors contributing to the summer 2003 European heatwave". In: *Weather* 59.8, pp. 217–223.

Burillo, Daniel et al. (2019). "Electricity infrastructure vulnerabilities due to long-term growth and extreme heat from climate change in Los Angeles County". In: *Energy Policy* 128, pp. 943–953.

Chen, Feng, Xuchao Yang, and Weiping Zhu (2014). "WRF simulations of urban heat island under hot-weather synoptic conditions: The case study of Hangzhou City, China". In: *Atmospheric research* 138, pp. 364–377.

Forzieri, Giovanni et al. (2018). "Escalating impacts of climate extremes on critical infrastructures in Europe". In: *Global environmental change* 48, pp. 97–107.

Frumkin, Howard (2016). "Urban sprawl and public health". In: *Public health reports.*

Heaviside, Clare, Helen Macintyre, and Sotiris Vardoulakis (2017). "The urban heat island: implications for health in a changing environment". In: *Current environmental health reports* 4.3, pp. 296–305.

Hu, Xiao-Ming and Ming Xue (2016). "Influence of synoptic sea-breeze fronts on the urban heat island intensity in Dallas–Fort Worth, Texas". In: *Monthly Weather Review* 144.4, pp. 1487–1507.

Jiang, Shaojing et al. (2019). "Amplified urban heat islands during heat wave periods". In: *Journal of Geophysical Research: Atmospheres* 124.14, pp. 7797–7812.

Li, Dan and Elie Bou-Zeid (2013). "Synergistic interactions between urban heat islands and heat waves: The impact in cities is larger than the sum of its parts". In: *Journal of Applied Meteorology and Climatology* 52.9, pp. 2051–2064.

Madrigano, Jaime et al. (2015). "A case-only study of vulnerability to heat wave–related mortality in New York City (2000–2011)". In: *Environmental health perspectives* 123.7, pp. 672–678.

McEvoy, Darryn, Iftekhar Ahmed, and Jane Mullett (2012). "The impact of the 2009 heat wave on Melbourne's critical infrastructure". In: *Local Environment* 17.8, pp. 783–796.

Miralles, Diego G et al. (2014). "Mega-heatwave temperatures due to combined soil desiccation and atmospheric heat accumulation". In: *Nature geoscience* 7.5, pp. 345–349.

Peng, Roger D et al. (2011). "Toward a quantitative estimate of future heat wave mortality under global climate change". In: *Environmental health perspectives* 119.5, pp. 701–706.

Ramamurthy, P and E Bou-Zeid (2017). "Heatwaves and urban heat islands: a comparative analysis of multiple cities". In: *Journal of Geophysical Research: Atmospheres* 122.1, pp. 168–178.

Stéfanon, Marc et al. (2014). "Soil moisture-temperature feedbacks at meso-scale during summer heat waves over Western Europe". In: *Climate dynamics* 42.5, pp. 1309–1324.

Zhao, Lei et al. (2018). "Interactions between urban heat islands and heat waves". In: *Environmental research letters* 13.3, p. 034003.

Zuo, Jian et al. (2015). "Impacts of heat waves and corresponding measures: a review". In: *Journal of Cleaner Production* 92, pp. 1–12.

Figures

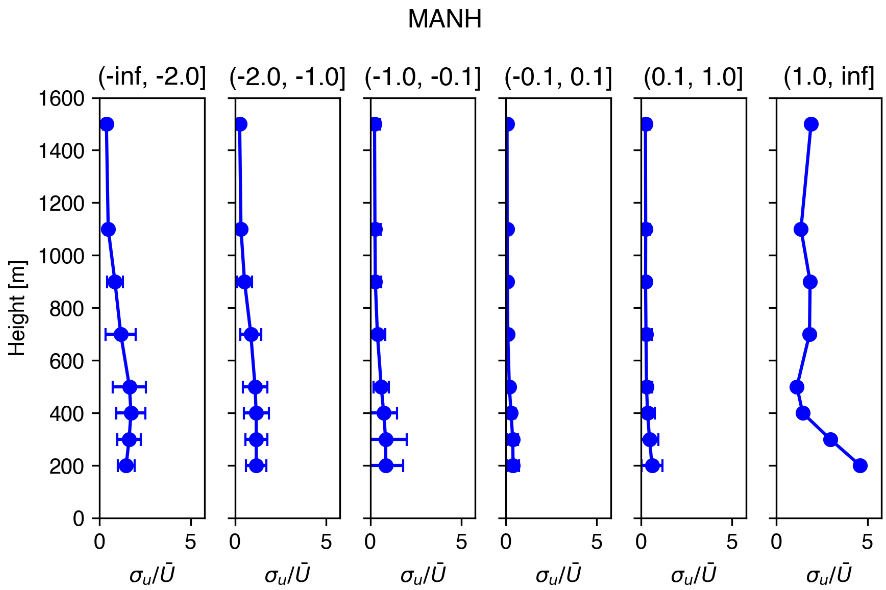

Figure 1: Vertical profiles of turbulent intensity for the zonal wind component in Manhattan, averaged over surface stability classes. Error bars show 1 standard deviation from the mean.

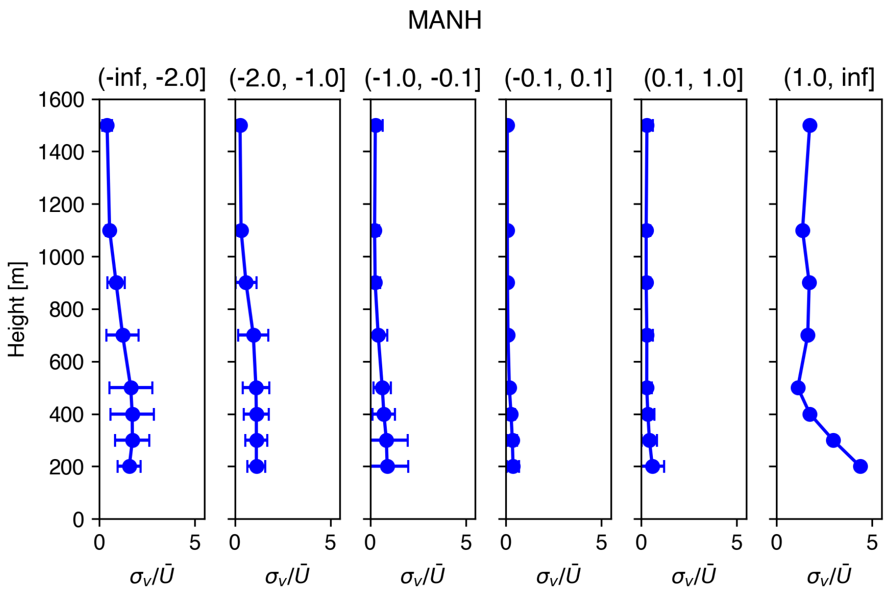

Figure 2: As in Figure 1 for the meridional wind component.

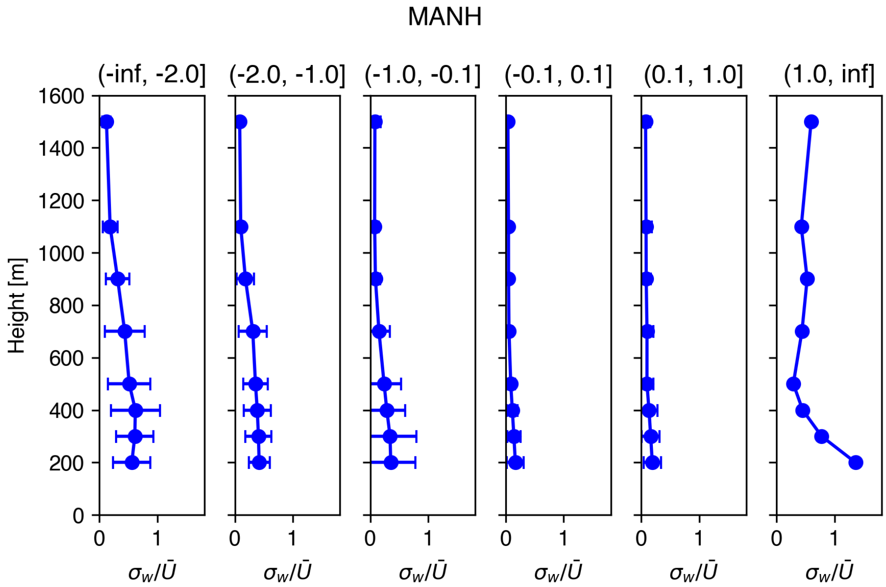

Figure 3: As in Figure 1 for the vertical velocity component.

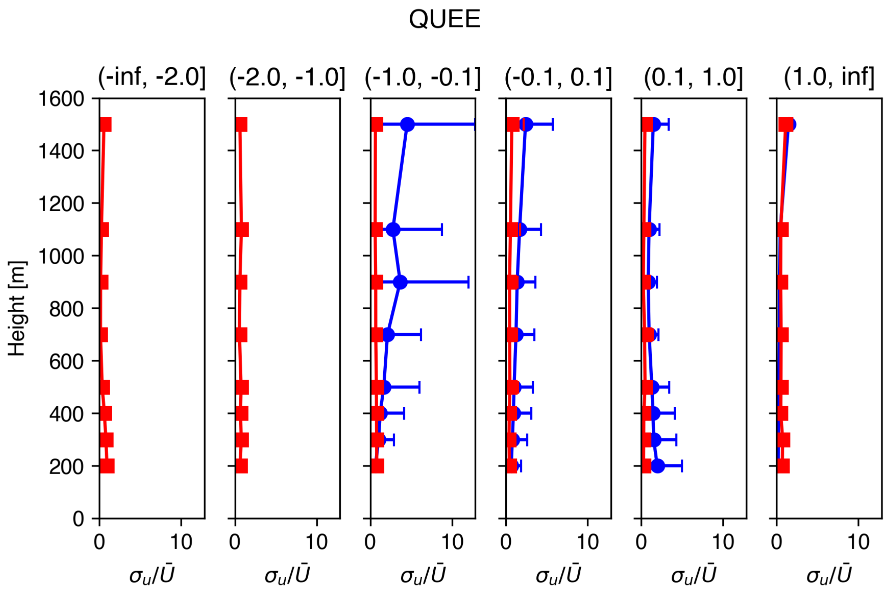

Figure 4: Vertical profiles of turbulent intensity for the zonal wind component in Queens, averaged over surface stability classes for normal and extreme heat event days. Error bars show 1 standard deviation from the mean.

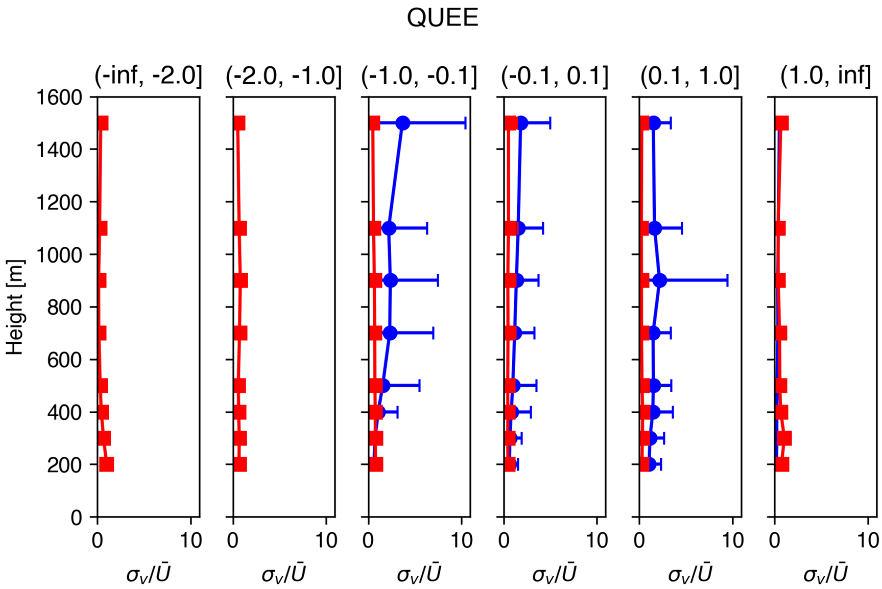

Figure 5: As in Figure 4 for the meridional wind component.

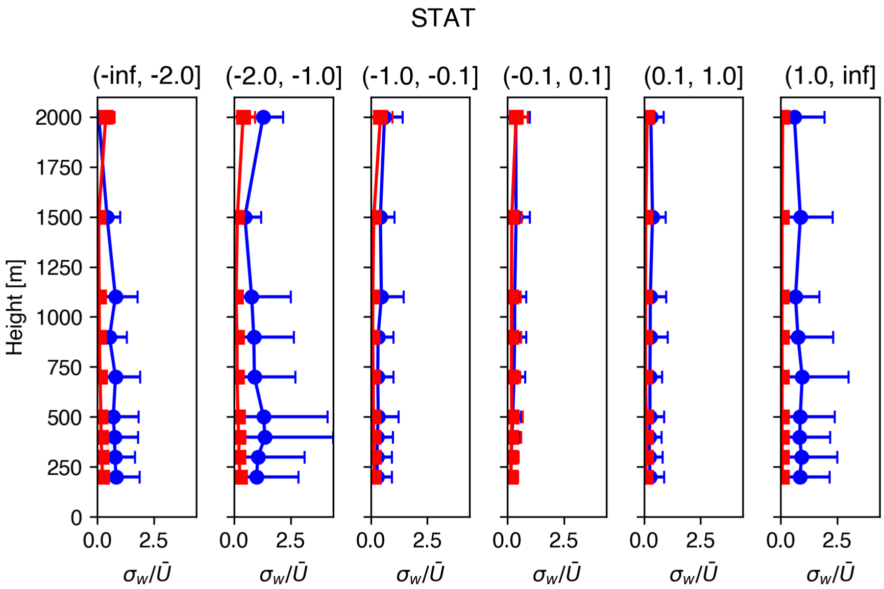

Figure 6: As in Figure 4 for the vertical velocity component.

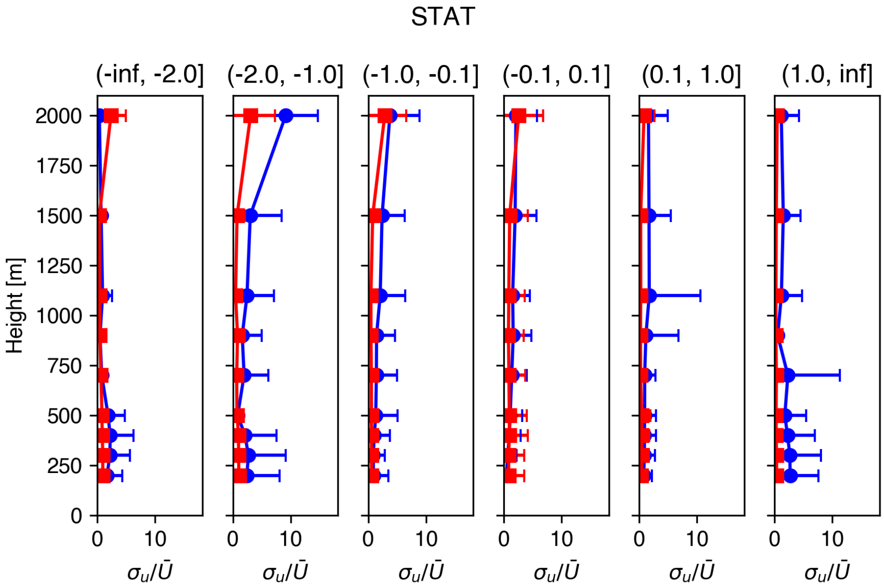

Figure 7: Vertical profiles of turbulent intensity for the zonal wind component in Staten Island, averaged over surface stability classes for normal and extreme heat event days. Error bars show 1 standard deviation from the mean.

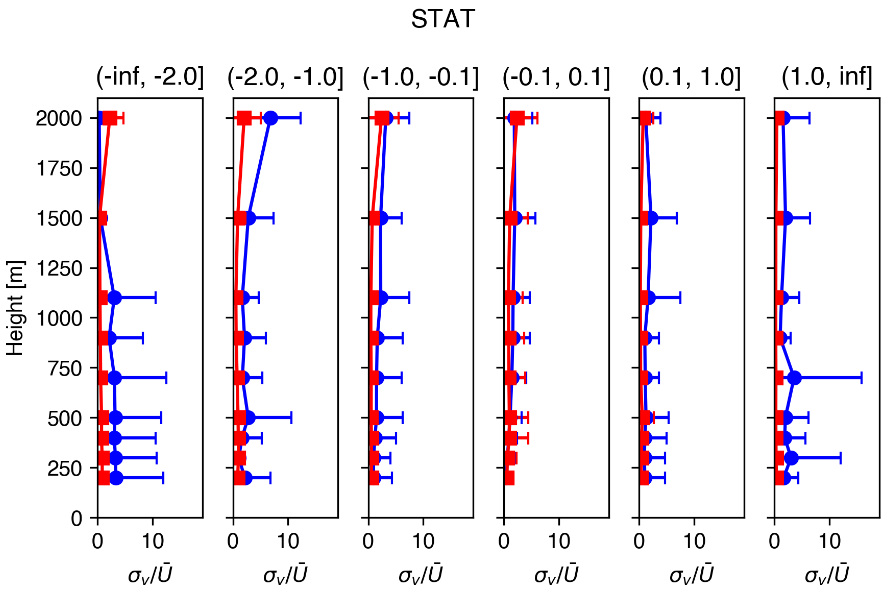

Figure 8: As in Figure 7 for the meridional wind component.

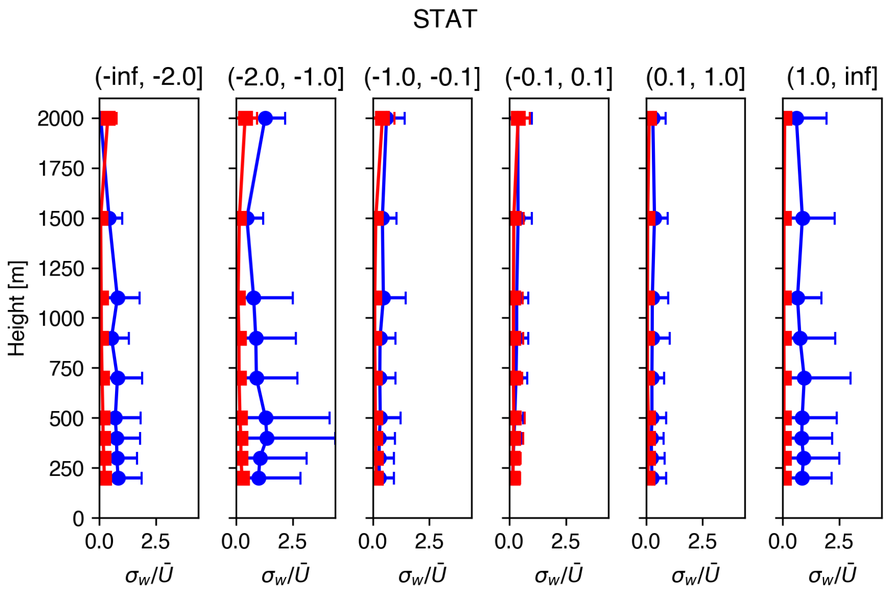

Figure 9: As in Figure 7 for the vertical velocity component.

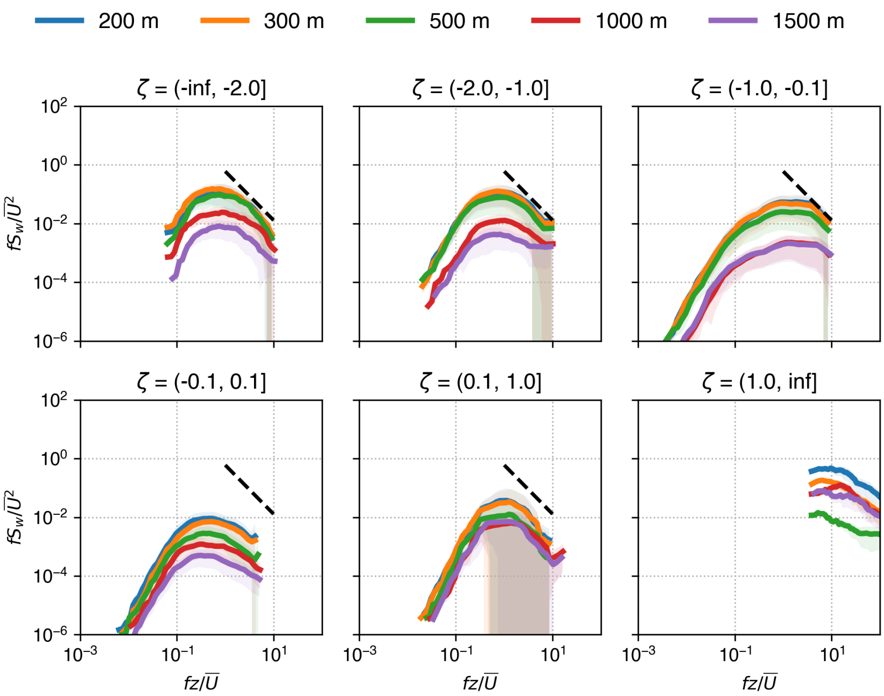

Figure 10: Normalized power spectra of vertical velocity components at multiple heights in Manhattan, grouped by stability class. -2/3 line shown for reference over the inertial subrange.

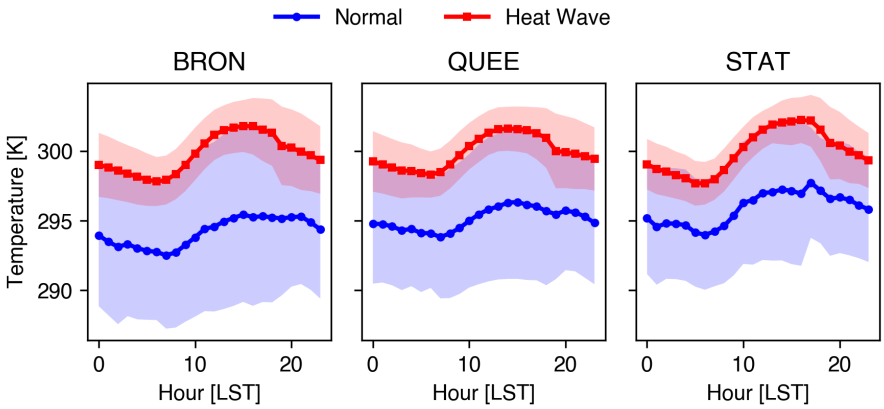

Figure 11: .

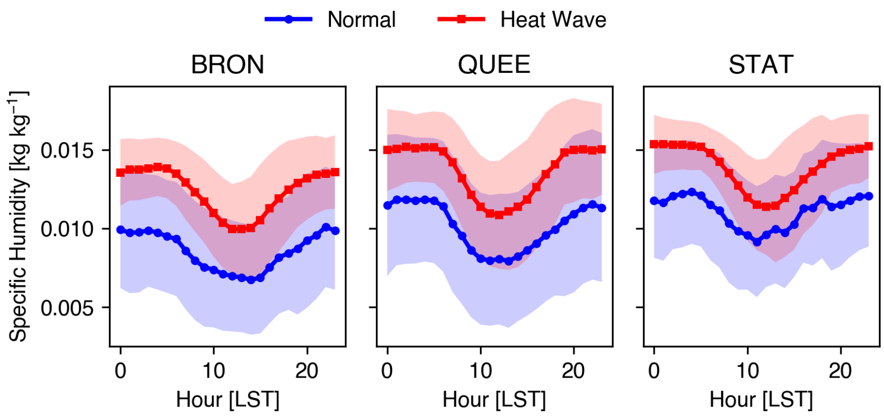

Figure 12: .

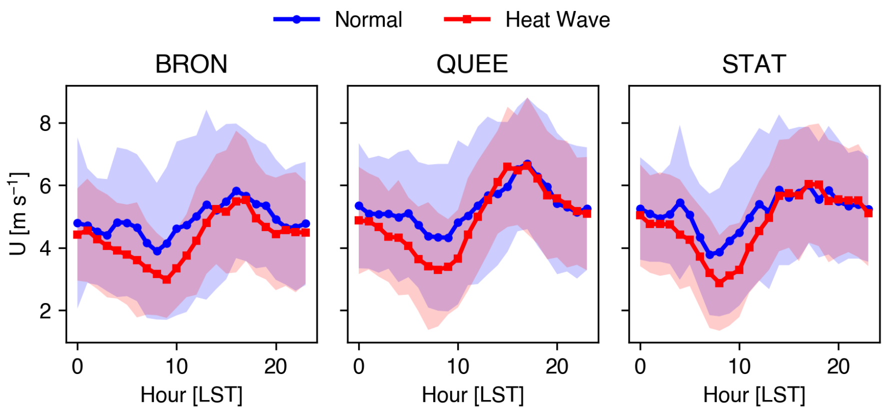

Figure 13: .

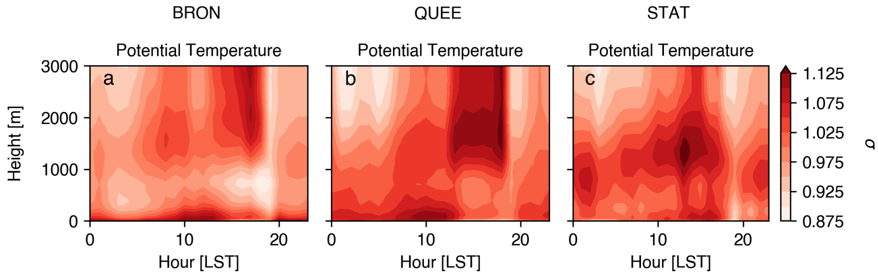

Figure 14: .

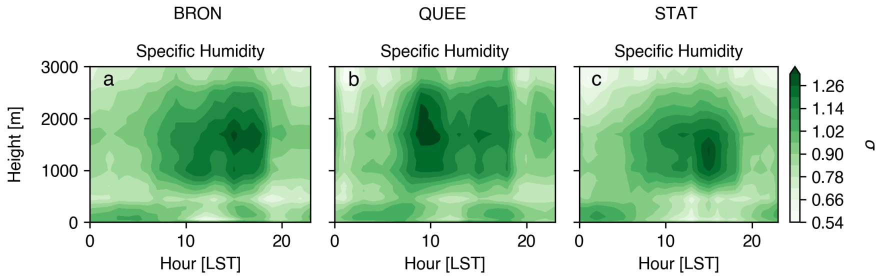

Figure 15: .

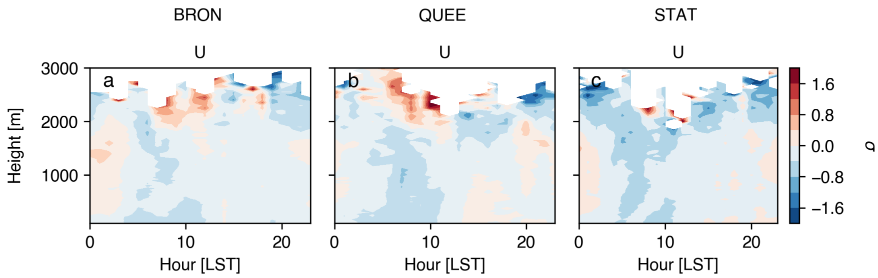

Figure 16: .

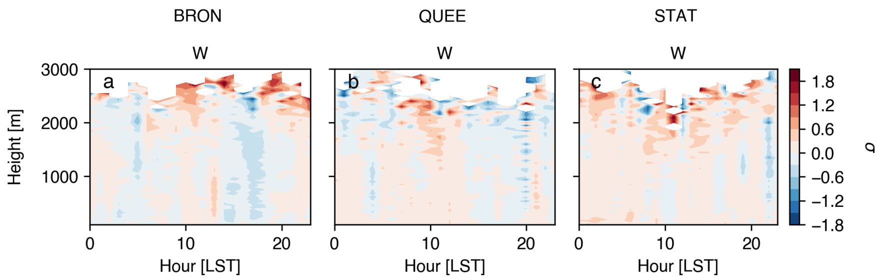

Figure 17: .

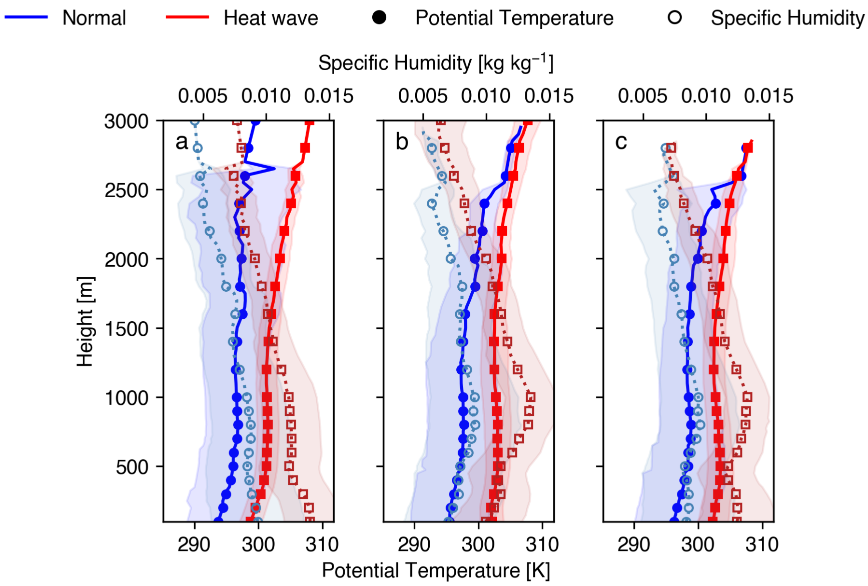

Figure 18: .

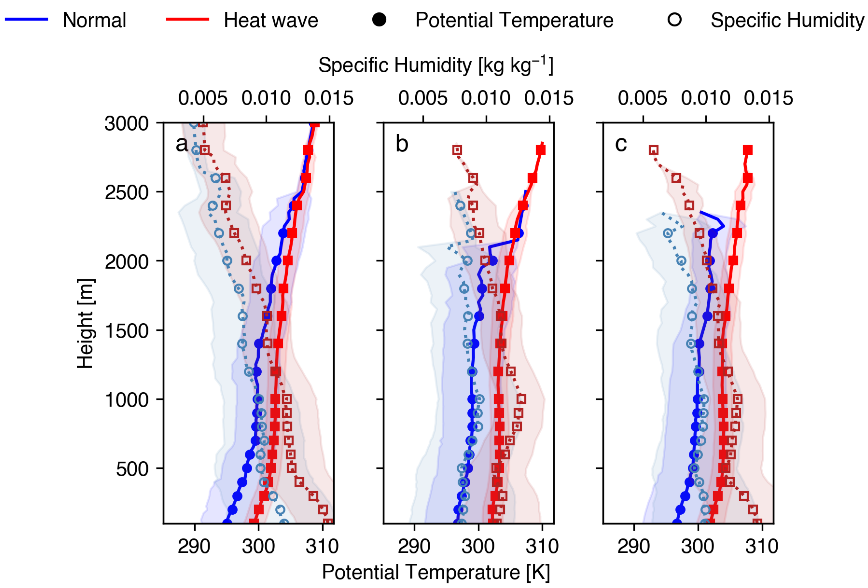

Figure 19: .

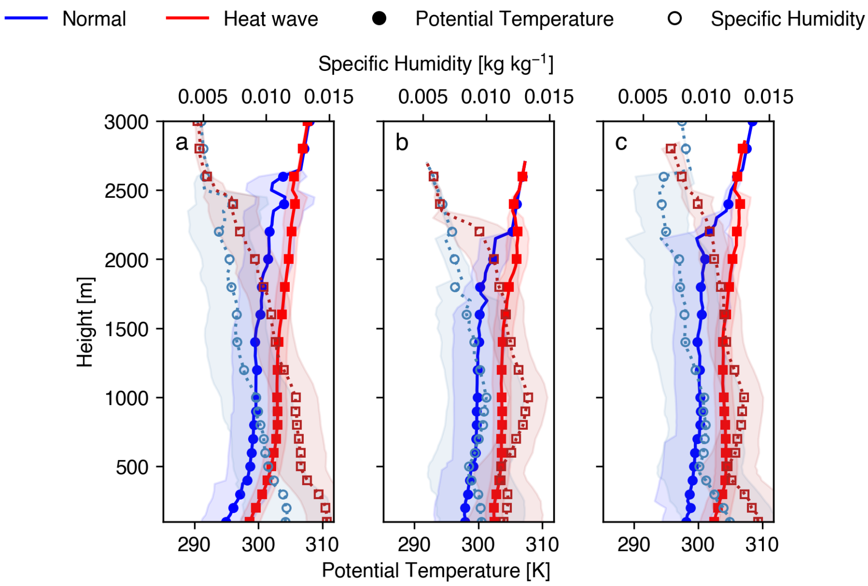

Figure 20: .

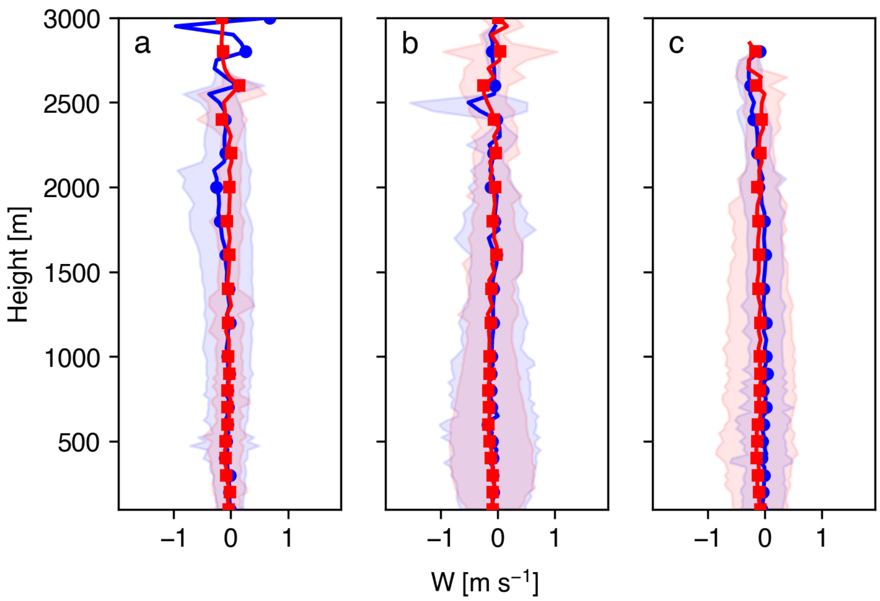

Figure 21: .

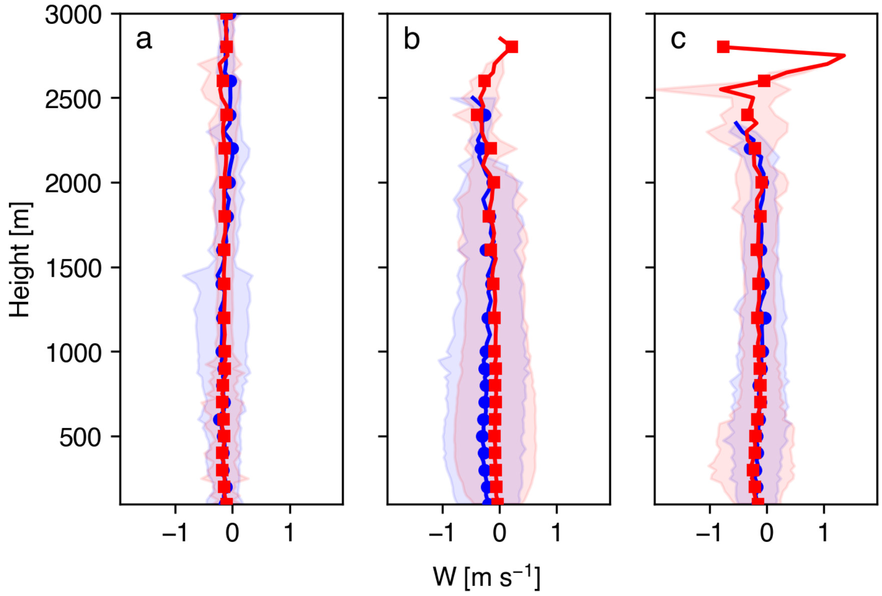

Figure 22: .

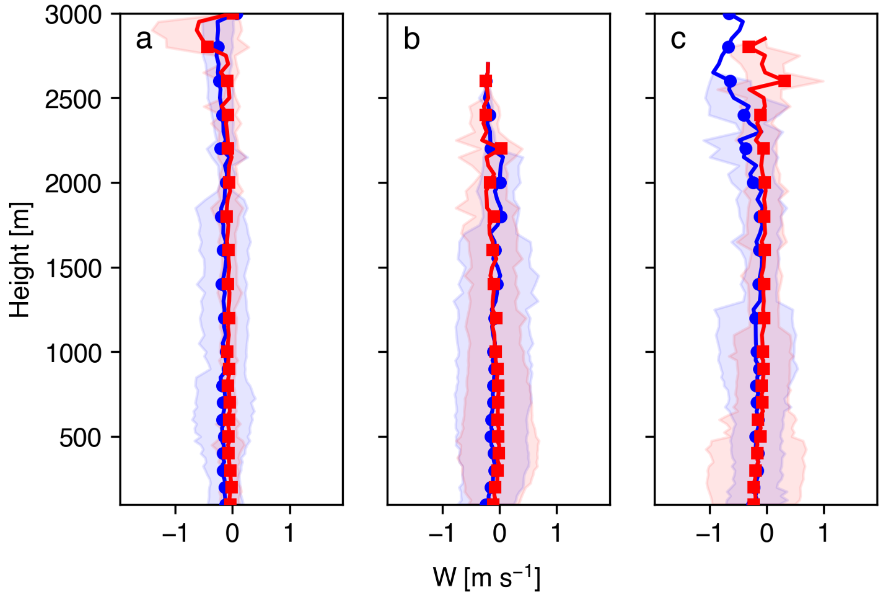

Figure 23: .